

Article

Upgrading a Shrouded Wind Turbine with a Self-Adaptive Flanged Diffuser

Jun-Feng Hu ¹ and Wen-Xue Wang ^{2,*}

¹ Department of Aeronautics and Astronautics, Engineering School, Kyushu University, Motooka, Nishi-ku, Fukuoka 819-0395, Japan; E-Mail: hu-junfeng@riam.kyushu-u.ac.jp

² Research Institute for Applied Mechanics, Kyushu University, Kasuga, Fukuoka 816-8580, Japan

* Author to whom correspondence should be addressed; E-Mail: bungaku@riam.kyushu-u.ac.jp; Tel.: +81-92-583-7757; Fax: +81-92-583-7760.

Academic Editor: Frede Blaabjerg

Received: 10 April 2015 / Accepted: 26 May 2015 / Published: 3 June 2015

Abstract: In this paper, a self-adaptive flange is proposed for the wind turbine shrouded by a flanged diffuser to reduce the wind loads acting on the flanged diffuser at high wind velocities. The self-adaptive flange can maintain the advantages of the flanged diffuser at wind velocities lower than the rated velocity and reduce the wind loads acting on the diffuser and blades at higher wind velocities. Numerical analyses of fluid-structure interactions are carried out to investigate the flow field around the diffuser with a self-adaptive flange and the variation of wind load acting on the diffuser due to the reconfiguration of the self-adaptive flange at various wind velocities. Numerical results show that the wind load acting on the total flanged diffuser can be reduced by about 35% at 60 m/s due to the reconfiguration of the self-adaptive flange.

Keywords: wind turbine; self-adaptive flange; diffuser; drag reduction; fluid-structure interaction

1. Introduction

With the growing concern about the issues of increasing energy consumption and global climate change, the development of clean and sustainable energy sources has attracted more and more attention in the whole world. Wind energy is one of the most important sustainable energy sources, and wind

turbine systems are an important way to extract the energy from wind. It is known that the power extractable from the wind by a wind turbine increases with the cube of the wind velocity so that even small increase in wind velocity can lead to a large increase in wind power generation. Therefore, many researchers have been making efforts to develop new technologies that can effectively accelerate the approaching wind velocity. One of advanced wind turbine designs is the diffuser augmented wind turbine (DAWT). It was first proposed by Lilley and Rainbird in 1956 [1]. Experimental studies were then carried out by Oman *et al.* [2], Igra [3,4], Foreman and Gilbert [5], Phillips *et al.* [6]. These experimental results proved that the DAWT can extract much more power from the wind than any similar bare wind turbine with the same rotor diameter. Afterwards, many theoretical and numerical studies [7–12] have been performed to investigate and improve the performance of DAWTs. Most of these researches presented similar conclusions with early experimental results. The results from Hasen [7] showed that the power coefficient of the wind turbine with a wing profiled shroud is 1.8 times that of a bare wind turbine. Similarly, Bet and Grassmann reported that about a 2-fold power augmentation was achieved by using two wing profiled rings mounted around the rotor [8]. Computational fluid dynamics (CFD) analysis for a shrouded wind turbine with a simple frustum diffuser was carried out by Jafari [9]. The shrouded wind turbine improved the power extraction over a bare turbine by nearly 1.7 times. Van Bussel [10] demonstrated two power coefficients based on the rotor swept area and the diffuser exit area, and indicated that the power coefficients of almost all the DAWTs reported based on the diffuser exit area are less than the Betz limit, although the power coefficients based on the rotor swept area are larger than the Betz limit. It was reported by Werle and Presz [11] that a thrust increase of nearly 80% above the bare turbine level is attainable with moderate diffusion and exit plane suction pressures. Jamieson [12] found that the ideal maximum power coefficient of DAWT based on the rotor swept area is $8/9$ which is 1.5 times the Betz limit.

In addition to the above research on DAWTs, Ohya *et al.* [13,14] developed a new shrouded wind turbine with a large flange mounted at the exit of the diffuser and a curved inlet section. A 3 kW wind turbine shrouded with a flanged diffuser and an illustration of the wind flow around the flanged diffuser are shown in Figure 1. They found that the large flange created a low-pressure region owing to the strong vortices formed behind the flange based on the wind tunnel tests. As a result, much more wind was drawn into the diffuser than in a general DAWT without the flange. Their experimental and numerical results showed that the flange increased the wind velocity in the nozzle of the diffuser by 1.6–2.4 times over the upwind velocity, and by 1.2–1.7 times over the wind velocity in the nozzle of the diffuser obtained by the same diffuser but without the flange, respectively. This acceleration effect of the wind velocity led to an increase in the power extraction by 2–3 times over the bare wind turbine and 1.4–2.1 times over the wind turbine with the same diffuser but without the flange, respectively. After that, extensive experiments and CFD simulations were carried out to investigate the effects of various geometrical parameters of the flanged diffuser on the flow field around the diffuser and the power coefficients [15–19]. It was reported in [17] that a 500 W wind turbine shrouded by a long flanged diffuser showed an increase in power output by 4–5 times compared to the bare wind turbine with the same rotor diameter. Several compact (short) flanged diffusers were investigated in [18], and the experiments revealed that a 5 kW flanged diffuser shrouded wind turbine obtained an augmentation in output power by 2.5 times compared to the bare wind turbine. It was further reported that the power coefficient based on the diffuser exit area is 0.54 which is still higher than that of the conventional

wind turbine without diffuser (0.4). Computations were performed by Mansour and Meskinkhoda [19] to investigate the flow fields around the flanged diffuser and their numerical results were consistent with those previously reported by Abe *et al.* [15]. It was further proved that the flange improve on-axis stream velocity at the inlet by 1.18 times over the wind turbine with the same diffuser but without the flange.

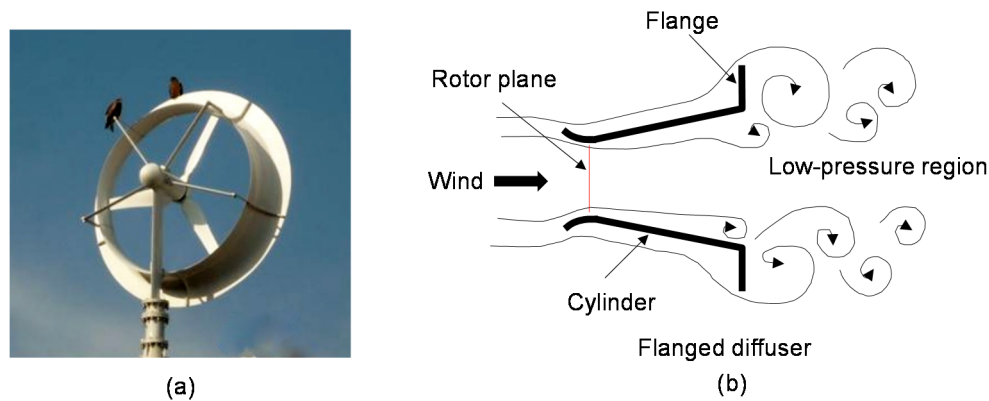


Figure 1. (a) A 3 kW wind turbine shrouded by a flanged diffuser and (b) illustration of wind flow around the flanged diffuser [17].

In addition to the above research in the flow field around the flanged diffuser, the influence of flanged diffuser on the dynamic behavior of rotating rotor blades of a 3 kW wind turbine with a compact flanged diffuser was investigated by wind tunnel experiments in a recent work [20]. It was found that the rotational speed of the blade of the wind turbine with a flanged diffuser is about 1.35 times that without the flanged diffuser, which led to higher strains at the root of the rotating blades of the wind turbine with a flanged diffuser than those in the rotating blades of the bare wind turbine with the same rotor. According to this recent research, issues involving the wind turbine structure are again recognized. In addition to the advantages, including the acceleration effect of wind velocity, low noise, and kindness to birds, the drawbacks of the wind turbine shrouded by a flanged diffuser are also obvious. An extra and large structure, namely, the flanged diffuser is added to a bare wind turbine, which makes this kind of wind turbine complicated and costly, especially for very large-scale wind turbines. It is easily imagined that a large flanged diffuser brings higher wind loads to the supporting structures of wind turbine than a bare wind turbine, although a large flange can lead to high wind velocity and then high wind power extraction. For this reason, it is difficult to develop very large-scale wind turbines with a flanged diffuser due to the structure and cost issues, although a large wind turbine is much more cost effective in wind power extraction than a small wind turbine. Thus, it is of interest to develop a smart flanged diffuser which can maintain the acceleration function at low wind velocities and meanwhile can reduce the wind loads at high wind velocities. This is a new challenge for upgrading wind turbines shrouded by flanged diffusers.

In this study, a diffuser with a self-adaptive flange is proposed based on a novel idea of bi-cantilevered plates. This self-adaptive flange not only can maintain the advantage of accelerating the approaching wind velocity at velocities lower than the rated wind velocity but also can gradually reduce the wind loads acting on the wind turbine structure at higher wind velocities. Furthermore, this proposed flange is completely self-adaptive and works without any aid of extra electrical or

mechanical device. That is, no electric energy is consumed for the control of this self-adaptive flange. Numerical analyses of fluid-structure interaction (FSI) are carried out to investigate the flow field around the diffuser with the self-adaptive flange and the variation of wind load acting on the diffuser due to the reconfiguration of the self-adaptive flange at various wind velocities.

2. A Novel Diffuser with a Self-Adaptive Flange

It is useful to recognize that how the wind load acts on the wind turbine shrouded by a flanged diffuser is affected by the flanged diffuser before considering a self-adaptive flange. According to the previous results [21] of wind tunnel experiments for a 500 W wind turbine with and without a flanged diffuser and CFD analysis using the CFD code of Star-CD, wind loads acting on a wind turbine with a typical compact flanged diffuser are about 3.2 times the wind loads acting on a bare wind turbine with the same rotor diameter, as shown in Figure 2. In the other words, about 69% of the total wind load acting on the wind turbine with a flanged diffuser is caused by the flanged diffuser. It is noted that in Figure 2 the towers of two kinds of wind turbines with and without flanged diffuser are assumed to have the same dimensions, although the tower of wind turbine with a flanged diffuser generally has larger diameter than that of a bare wind turbine because of higher wind load caused by the flanged diffuser. For this reason, a large-scale wind turbine with flanged diffuser requires a much more complicated and stronger supporting structure, including the tower and the supporting structure of flanged diffuser, than a bare wind turbine to assure the safety of the wind turbine at limited high wind velocity. As a result, a higher cost of a wind turbine with a flanged diffuser is inevitable. Therefore, it is important to reduce the wind load caused by the flanged diffuser for the development of large-scale and practicable wind turbine with a flanged diffuser.

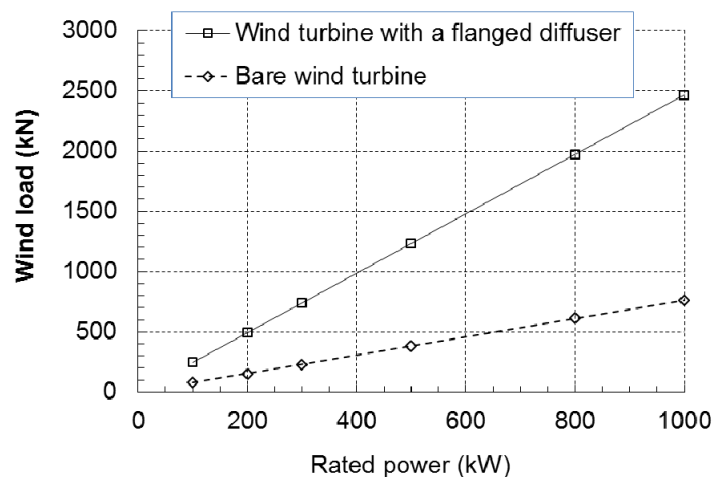


Figure 2. Wind loads acting on two kinds of wind turbines with and without a flanged diffuser at 60 m/s for various rated powers.

Referring to Figure 1, it is seen that the flanged diffuser consists of two main parts: cylindrical part and flange. Thus the wind load acting on the flanged diffuser can be divided into two parts: partial wind load caused by the cylindrical part and another partial wind load caused by the flange. In order to reduce the above wind loads significantly, challenges to the structures of these two parts are necessary. As a first trial, this study takes on the challenge of developing a smartly adaptive flange. Here a

smartly adaptive flange means that a flange which satisfies two requirements. The first one is that the flange can maintain the original function of accelerating the approaching wind at a velocity lower than a specified wind velocity and the second one is that the flange can reduce the wind load gradually with the increase of wind velocity at velocities higher than the specified velocity. In the present study, the rated velocity V_r of the wind turbine is considered as the specified wind velocity. Based on today's updated control technologies, it is not difficult to make a smartly adaptive flange using extra and active electric or mechanical control devices. However, extra and active electric and mechanical control devices not only further increase the manufacturing cost of the wind turbine, but also consume electric energy. Therefore, in present study, a self-adaptive flange which does not use any extra and active electric or mechanical devices, is considered. Learning from natural leaves of plant and trees tells us that a flexible flange structure can gradually reduce the wind load acting on it by its deformation, as illustrated in Figure 3. The flange in the conventional wind turbine with a flanged diffuser is rigidly connected with the cylindrical part and has a small deformation even at the limiting high wind velocity, which leads to a high wind load acting on the flange. In the above flexible flange idea, the flange is like a cantilevered plate with a fixed upper edge and a free lower edge so that it can gradually reduce the wind load acting on it by its deformation. However, this idea only satisfies the second requirement of a smartly adaptive flange and the first one is not satisfied because the flexible flange also deforms at wind velocities lower than the rated velocity V_r , as depicted by the solid curve in Figure 3c. A smartly adaptive flange requires that the open gap be zero or nearly zero at low wind velocities and gradually increase as wind velocity increases to high velocities. Therefore, improvement of the flexible flange idea is necessary to make a real smartly adaptive flange.

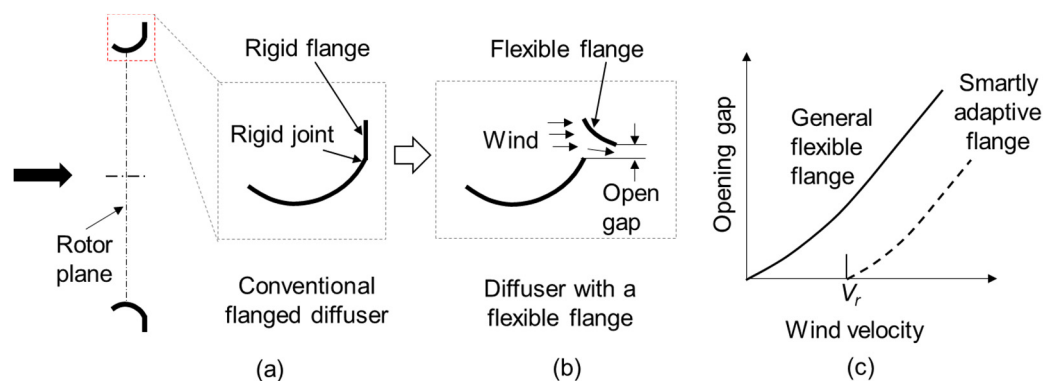


Figure 3. A general flexible flange idea: (a) conventional rigid flanged diffuser; (b) general flexible flange idea; (c) curves of open gap vs. wind velocity.

In order to overcome the shortcomings of the above flexible flange, a flexible flange idea consisting of two cantilevered plates is considered, as described in Figure 4. Two cantilevered plates may have different flexural rigidity, which depends on the design of the interval between two plates, on the length of the two plates, on the contact requirement at rated velocity, and on the gap opening at the limited high wind velocity. It is understood that the deformation of the rear plate is zero or nearly zero before the front plate contacts the rear plate because the wind load acting on the rear plate is negligible. Once the front plate contacts the rear plate, the rear plate will deform gradually together with the front plate with the increase of wind velocity due to the contact force. Obviously, this idea of a bi-cantilever

flange satisfies the two requirements mentioned above for a smartly adaptive flange and this bi-cantilever flange is a completely self-adaptive flange. As the deformation of the bi-cantilever flange is not controlled by any extra and active electric or mechanical devices but rather adapts passively to the wind load, in the study the bi-cantilever flange is named hereinafter a self-adaptive flange.

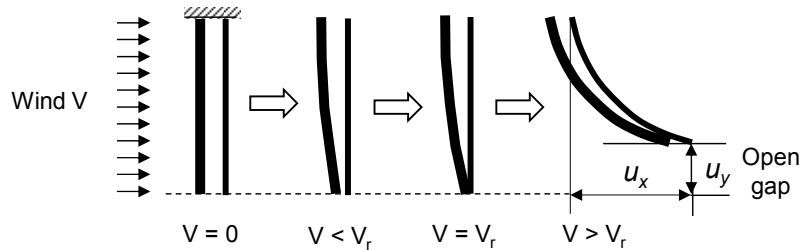


Figure 4. Illustration of the idea of a bi-cantilever flange.

A flanged diffuser with a self-adaptive flange is proposed based on the above self-adaptive flange concept. A 100 kW wind turbine with a typical compact-type flanged diffuser [21] is considered as a model in the present study. Geometry and dimensions of the compact-type flanged diffuser and the structure of self-adaptive flange are depicted in Figure 5. The outer diameter of the flange is 15.438 m, the height of the flange is 0.6475 m, the throat diameter of the cylindrical part is 12.95 m, and the length on the flanged diffuser in the flow direction is 1.777 m. In the case of original 100 kW unit built at the Ito campus of Kyushu University, the cylindrical part and the flange were made of a sandwich shell structure consisting of a glass fiber reinforced plastic (GFRP) skin and a porous plastic core. The thickness of the sandwich shell is about 30 mm, and the ribs were made of 9 mm in thickness steel plate.

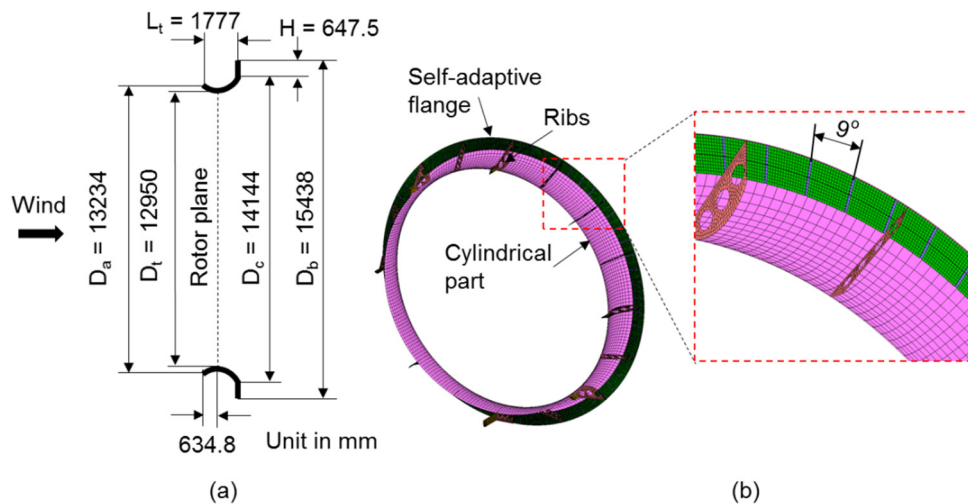


Figure 5. A compact-type flanged diffuser with a self-adaptive flange.

To simplify the present numerical simulation, the cylindrical part, ribs and other structural parts of the wind turbine are considered as rigid structures, and only the flange is considered a flexible structure. The flange is uniformly divided into 40 parts along the circumference and each one of the 40 parts is further equally divided into two subparts along the radial direction based on the original dimensions of the flange and the fabrication view of the subparts, as shown in Figure 5b. Two rings made of rectangular steel pipe are added in the outer and middle diameters of the flange to fix the

upper edges of all the subparts of the divided flange. The rings, ribs, and cylindrical part form a relatively rigid structure. Each subpart consists of two cantilevered plates. The details of the models used in the analyses of the structure and CFD are described in next section.

3. Numerical Simulations

To investigate the availability and feasibility of above proposed self-adaptive flange applied to the wind turbine with a flanged diffuser, numerical simulations of the interaction between wind flow and the self-adaptive flange are carried out based on the iterative analyses of CFD and structural mechanics. In the iterative calculations, CFD analysis gives the pressure acting on the flange and structure analysis gives the deformation of the flange. The flowchart of the iterative calculations of fluid-structure coupling is described in Figure 6.

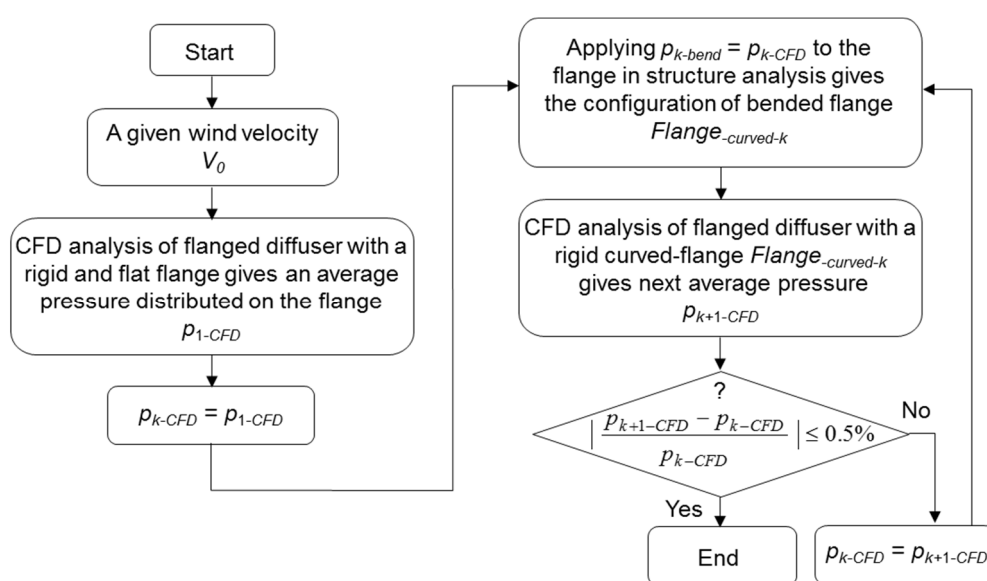


Figure 6. Flowchart of the iterative CFD and structure coupling analyses.

It is noted that, in general, the exact pressure acting on the flexible flange is quite complicated due to the interaction between the fluid and deformation of the flange and fluctuates around its mean value over time [20,22]. The pressure distribution on the flange near the outer and inner boundary of the flange is not uniform due to the influence of boundary conditions. However, on the other hand, according to the recent wind tunnel experiments [20], the fluctuation of total pressure acting on a flexible plate is about 5% of the mean pressure if the plate has the proper flexure rigidity. The regions with abrupt pressure change near the outer and inner diameters of the flange are about 5.3% and 6.7%, respectively, of the whole area of the plate surface so that the influence of non-uniform pressure on the deformation of the plate is limited. Therefore, in the present analysis it is assumed that the flexible flange in the uniform and steady wind flow is approximately under a quasi-static equilibrium state and the pressure acting on the flange is uniformly distributed on the front surface of the flange. Here, the quasi-static equilibrium state means that the deformed flange in the flow is like a rigid curved-flange under this state. The iterative analyses of CFD and structure mechanics is completed if the difference between the two averaged pressures, namely, the pressure applied to the flat flange in structure analysis to solve the configuration of deformed curved-flange and that obtained from the CFD analysis of the

curved-flange, is less than 0.5%. Details of structure and CFD analyses are described in the following subsections. It is pointed that the more advanced FSI method of coupling simultaneously unsteady CFD with structural dynamics and moving objects using the immersed boundary method [23] is useful in further FSI analysis to obtain more accurate evaluation for the present flexible self-adaptive flange.

3.1. Structural Mechanics Analysis

According to the symmetry of the flange structure with respect to the rotor central axis, one of the 40 parts is used as the flange model in the structural mechanics analysis of the self-adaptive flange and its geometry and dimensions are described in Figure 7.

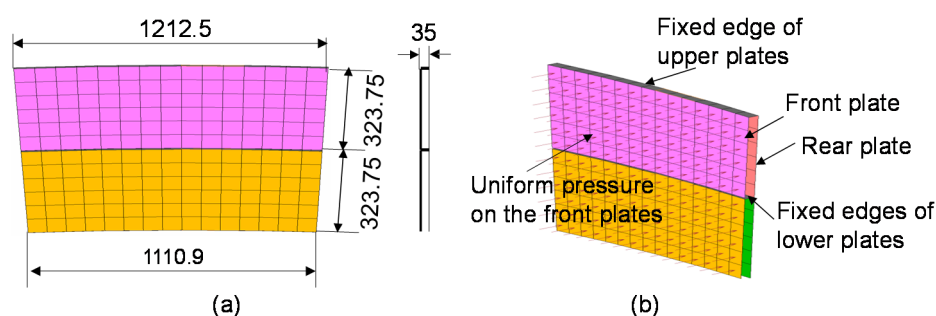


Figure 7. Self-adaptive flange model used in the structure analysis: (a) front view and dimensions; (b) 3-dimensional view and loading and boundary conditions.

One subpart consists of two cantilevered plates with fixed upper edges and free lower edges. Plates are sectorial and the widths of upper and lower arcs are about 1.111 m and 1.213 m, respectively. The length of plates is about 0.324 m. The thickness is 1.25 mm for the front plate and 0.5 mm for the rear plate, as given in Table 1.

Table 1. Stacking sequences and thickness of the front and rear plates.

Plate	Layers	Thickness (mm)	Stacking Sequence
Front plate	10	1.25	$[45/90/-45/0/45]_s$
Rear plate	4	0.5	$[75/-75]_s$

The pressure obtained from CFD analysis is uniformly applied on the front plates of the flange model and frictionless contact condition is defined between the front and rear plates. Carbon fiber reinforced plastic (CFRP) laminates are used for the front and rear plates since the laminate flexure rigidity is easily adjusted by changing the fiber direction of plies [24]. The CFRP laminates consist of multiple unidirectional CFRP laminas. The material properties of the unidirectional CFRP lamina are listed in Table 2.

Table 2. Material properties of the unidirectional CFRP lamina.

Young's Modulus (GPa)	Poisson's Ratio	Shear Modulus (GPa)
$E_1 = 142$	$\nu_{12} = 0.32$	$G_{12} = 4.2$
$E_2 = 8.8$	$\nu_{23} = 0.27$	$G_{23} = 3.7$
$E_3 = 8.8$	$\nu_{31} = 0.02$	$G_{31} = 4.2$

The stacking sequence and thickness of the front and rear plates are determined according to the conditions required by the proposed self-adaptive flange. That is, the front plate must be not in contact with the rear plate at $V < V_r$, be in contact with the rear plate at $V \geq V_r$, and the open gap (Figure 4) gradually increases with the increase of wind velocity at $V > V_r$. Based on the numerical calculations of fluid-structure interaction at a given rated wind velocity V_r , the stacking sequence and thickness of the front and rear plates are obtained and listed in Table 1. Nonlinearity of the finite deformation of the flange plates is considered in the structure mechanics analysis by nonlinear finite element method (FEM) and the numerical analysis is performed using commercially available codes of MSC/Marc2010. It is noted that the rated velocity $V_r = 12$ m/s is used in the present simulations hereafter.

3.2. CFD Analysis

According to the structural symmetry of the flanged diffuser, an axisymmetric model of flanged diffuser is used in the iterative CFD analyses. Computational domains for the model of a flanged diffusers with a rigid and flat flange is described in Figure 8a. A typical model of a flanged diffuser with a deformed self-adaptive flange is described in Figure 8b. Grids around two flanged diffusers are also depicted in Figure 8, respectively. It is noted that the bent shapes of two front plates of the self-adaptive flange are used as the configuration of the deformed flange in Figure 8b. The diffuser with a rigid and flat flange shown in Figure 8a is used in the first CFD analysis to solve the averaged pressure acting on the flange for the following structure analysis. After the first CFD analysis, applying the averaged pressure obtained from CFD analysis to the self-adaptive flange before deformation and conducting structure analysis solve a configurations of deformed self-adaptive flange. Next, the deformed self-adaptive flange is considered as a rigid curved-flange and is used in the next CFD analysis, as shown in Figure 8b, to solve the averaged pressure acting on the deformed self-adaptive flange for the next structure analysis. Repeat these iterative CFD and structure analyses until the convergent condition is satisfied, as described in the flowchart in Figure 6. In the CFD analyses, a uniform and steady flow V is set at the inlet boundary, no-slip boundary condition is specified on the surface of the flanged diffuser and the y^+ values are in the range of 23 to 381, zero-pressure condition is prescribed at the outlet boundary, slip boundary condition is applied to the top boundary, and axisymmetric condition is applied to the bottom boundary (the axisymmetric axis). The flow field is expressed by the continuity and incompressible Reynolds-averaged Navier–Stokes equations, the standard k – ε model is used in the analysis of turbulent flow, and a second-order numerical scheme is used to compute the convection and diffusion terms. Iterative CFD analyses are performed using a CFD code of ANSYS Fluent 13.0 which is a useful CFD code for modeling fluid flow in complex geometry. During the CFD analysis Reynolds number Re , turbulence intensity I , turbulent kinetic energy k , dissipation rate of turbulent kinetic energy ε , and the turbulent length scale l expressed by following equations, respectively, are used [25]:

$$Re = \frac{\rho V D_t}{\mu} \quad (1)$$

$$I = 0.16 \times Re^{-0.125} \quad (2)$$

$$k = 1.5 \times (VI)^2 \quad (3)$$

$$l = 0.07 D_t \quad (4)$$

$$\varepsilon = C_\mu^{3/4} \times \frac{k^{3/2}}{l} \quad (5)$$

where ρ ($= 1.225 \text{ kg/m}^3$) is the density of air, and μ ($= 1.8 \times 10^{-5} \text{ Pa} \cdot \text{s}$) is the viscosity coefficient of air at $20 \text{ }^\circ\text{C}$. $C_\mu \approx 0.09$ is the empirical constant specified in the turbulent model. The standard near wall function is chosen for the near wall treatment method with 10^{-6} of the convergence criterion.

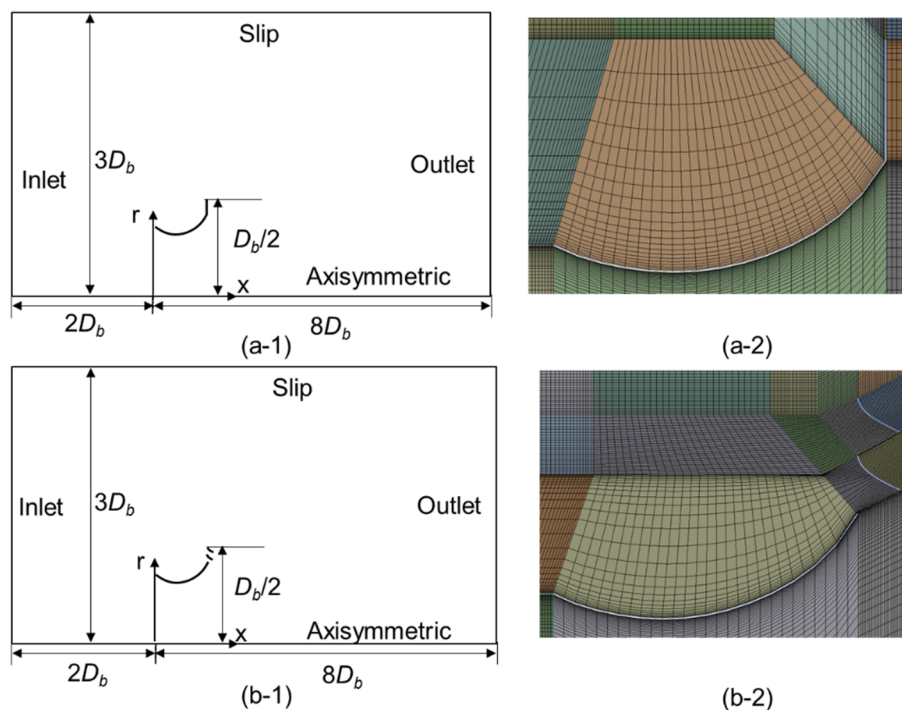


Figure 8. Computational domains, boundary conditions and grids: **(a-1)** diffuser with a rigid and flat flange; **(a-2)** related grids around the flanged diffuser; **(b-1)** diffuser with a typical deformed self-adaptive flange; **(b-2)** related grids around the flanged diffuser.

To investigate the effect of grid number and Reynolds number on the simulation results of distributions of velocity and pressure coefficient along the axisymmetric axis, two different grid systems and two different Reynolds numbers were investigated firstly in the CFD analysis using the flanged diffuser model shown in Figure 8a. In addition, for a further confirmation of the numerical accuracy of present CFD analysis, a comparative simulation is conducted for the model of a rigid flanged diffuser used in a previous research [16], as shown in Figure 9. The boundary conditions, the grid number, and the grid distribution are as same as those used for the CFD analysis of model shown in Figure 8a. V_0 is the approaching wind velocity of a uniform and steady flow at the inlet.

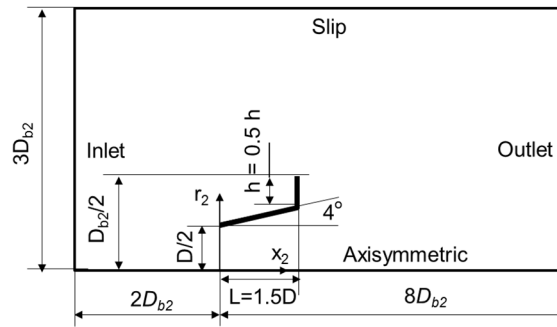


Figure 9. Computational domain used by a previous research [16] for the comparative simulation ($V_0 = 5 \text{ m/s}$, $D = 0.2 \text{ m}$).

4. Results and Discussion

Effects of grid number and Reynolds number on the simulation results are presented in Figure 10. The distribution of streamwise velocity and the pressure coefficient C_p along the axisymmetric axis are depicted in Figure 10a,b for two grid numbers (38,770 and 66,520) and two Reynolds numbers (10,634,703 and 53,173,516), respectively. Here, C_p is defined by:

$$C_p = (p - p_\infty) / (0.5\rho V_0^2) \tag{6}$$

where V_0 is the approaching wind velocity of a uniform and steady flow at the inlet, p is the static pressure along the axisymmetric axis, and p_∞ is the static pressure in a far upstream field. The transverse axis $x/D_b = \text{zero}$ denotes position of the entrance of the diffuser. As seen in the figure, the difference between the results of two different grid numbers or two different Reynolds numbers is not significant. In addition, the difference between two drag coefficients for grid numbers 38,770 and 66,520 with $Re = 10,634,703$ is about 1.6%. Therefore, all the following simulations use the grid number of 66,520. Numerical results of the comparative simulation are presented together with those obtained from the previous research [16] in Figure 11. The difference of both results is within about 5%, which confirms the accuracy of the present CFD analysis.

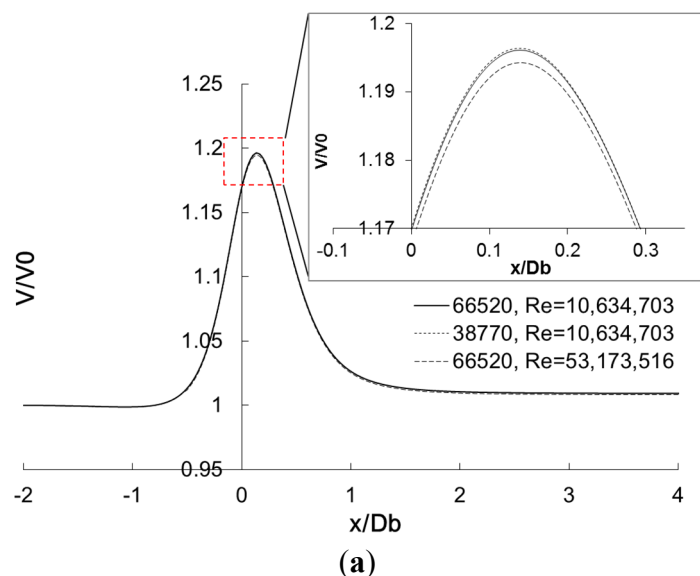


Figure 10. Cont.

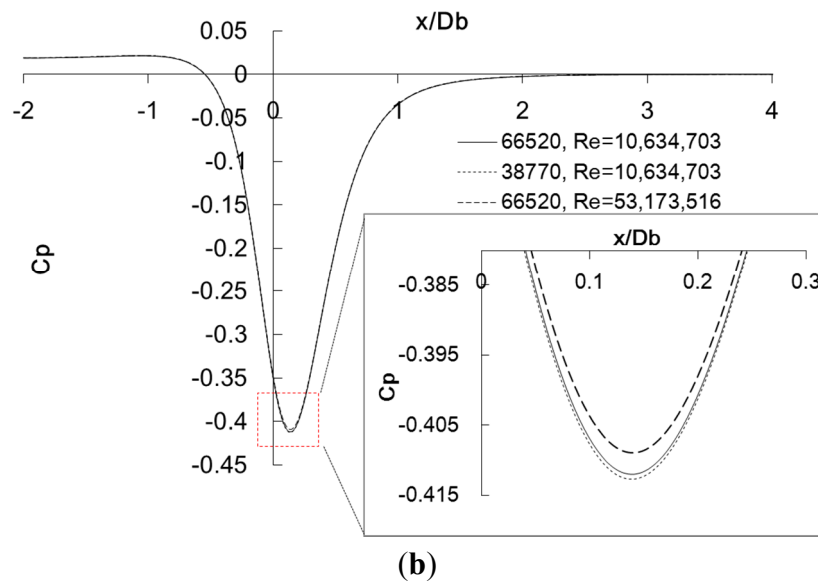


Figure 10. Effects of grid number and Reynolds number on the distributions of streamwise velocity and pressure coefficient along the axisymmetric axis in the case of the diffuser with a rigid and flat flange (Figure 8a): **(a)** streamwise velocity and **(b)** pressure coefficient.

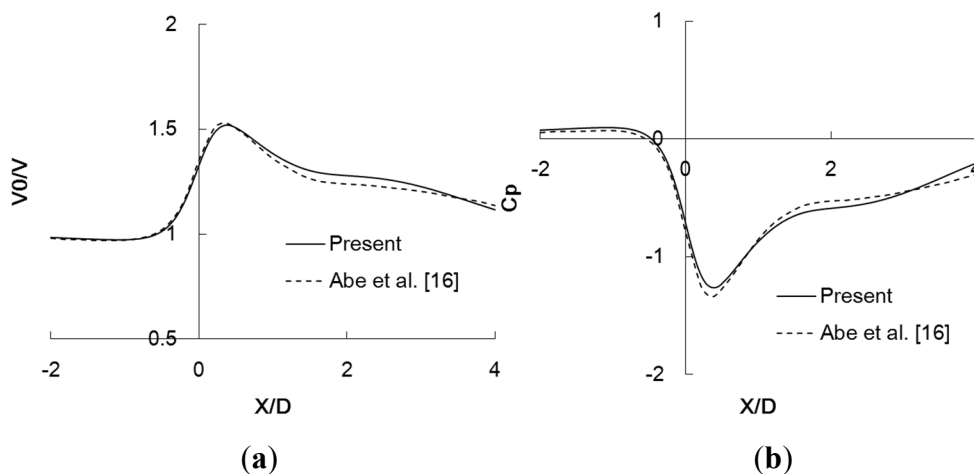


Figure 11. Streamwise velocity and pressure coefficient along the axisymmetric axis in the present comparative simulation are compared with those obtained from the previous research Abe *et al.* [16] ($V_0 = 5$ m/s, $D = 0.2$ m, $L = 1.5D$, $h = 0.5D$, $\phi = 4^\circ$): **(a)** streamwise velocity and **(b)** pressure coefficient.

Figure 12 presents the comparison of the drag forces and the drag coefficients along the flange, the cylindrical part and the total flanged diffuser obtained from the CFD analyses for the diffuser with a rigid and flat flange (Figure 8a) at various velocities. The drag coefficient is defined by:

$$C_d = drag / (0.5\rho V^2 A), \quad A = \pi D_b^2 / 4 \tag{7}$$

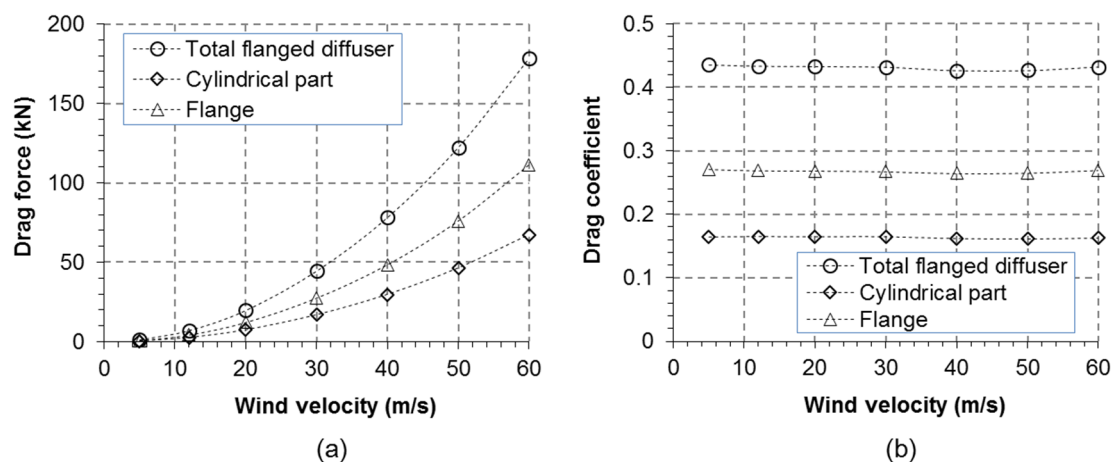


Figure 12. Comparison of the drag forces (a) and drag coefficients (b) among the flange, the cylindrical part, and the total flanged diffuser obtained from the CFD analyses for the diffuser with a rigid and flat flange (Figure 8a) at various velocities.

The reference area A is the circular area of outer diameter of the flange [21]. The relationship between the drag force and the velocity obeys the parabolic law. It is seen that about 60% of the total drag acting on the flanged diffuser is deduced from the flange. Numerical results of flow field (velocity contour and streamline) around the diffuser with a rigid and flat flange (Figure 8a) at 60 m/s are presented in Figure 13. It is seen in Figure 13a that acceleration of the wind velocity occurs in the inner region of the flanged diffuser, especially near the wall of the diffuser, although the velocity does not change so much in the radial direction. Since the power output is proportional to cube of the wind velocity as mentioned before, significant augmentation of power output is expectable. In addition, as seen in Figure 13b, two vortices are generated behind the flange, which cause a low-pressure region behind the flange and increase the pressure difference between the entrance and exit of the flanged diffuser. These results are consistent with those reported in [15,16]. The streamlines converge near the entrance of diffuser as indicated by the arrow, and more air is drawn into the diffuser.

Numerical results related to the flanged diffuser with a self-adaptive flange are presented in Figures 14–18. Velocity contour and streamline around the diffuser with the bended self-adaptive flange at 60 m/s are shown in Figure 14. Compared to Figure 13, it is seen that the velocity in the velocity field of Figure 14 is relatively lower than that in Figure 13 because the deformed self-adaptive flange allows partial wind to flow through the open gaps. Consequently, the acceleration effect of flanged diffuser decreases and the reduction in the wind load acting on the flanged diffuser and on the wind turbine blades are expectable due to the open gaps of the deformed self-adaptive flange. Similar behaviors are seen from the streamline field shown in Figure 14b. The streamlines at the entrance of flanged diffuser in Figure 14b become smoother than those in Figure 13, a lot of streamlines flow through the open gaps, and the separation region behind the flange is much smaller than that in Figure 13. As a result, the pressure difference between the entrance and exit of the diffuser decreases as the open gaps gradually become large and the wind drawn into the diffuser is less than that in Figure 13.

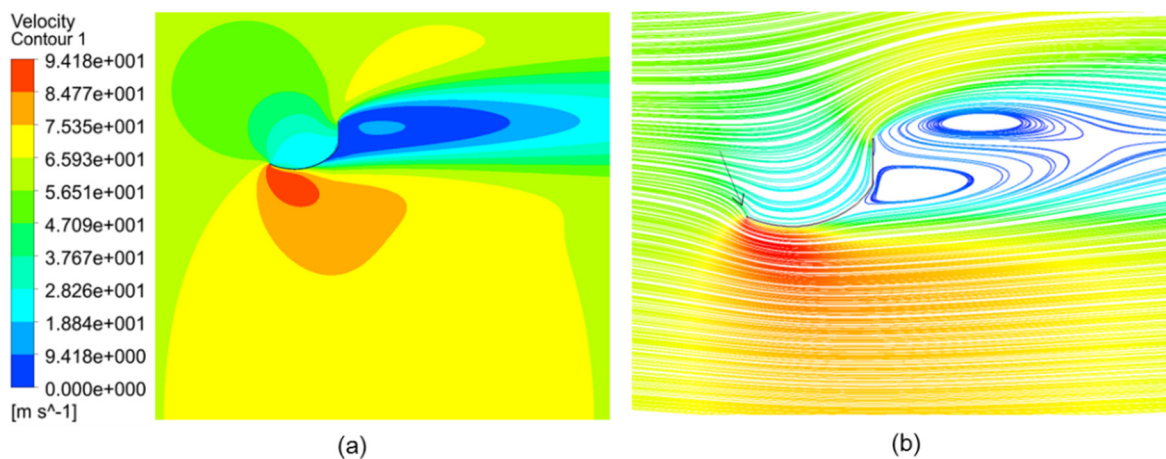


Figure 13. Flow fields around the flanged diffuser with a rigid flange (Figure 8a) at 60 m/s: (a) velocity contour and (b) streamline.

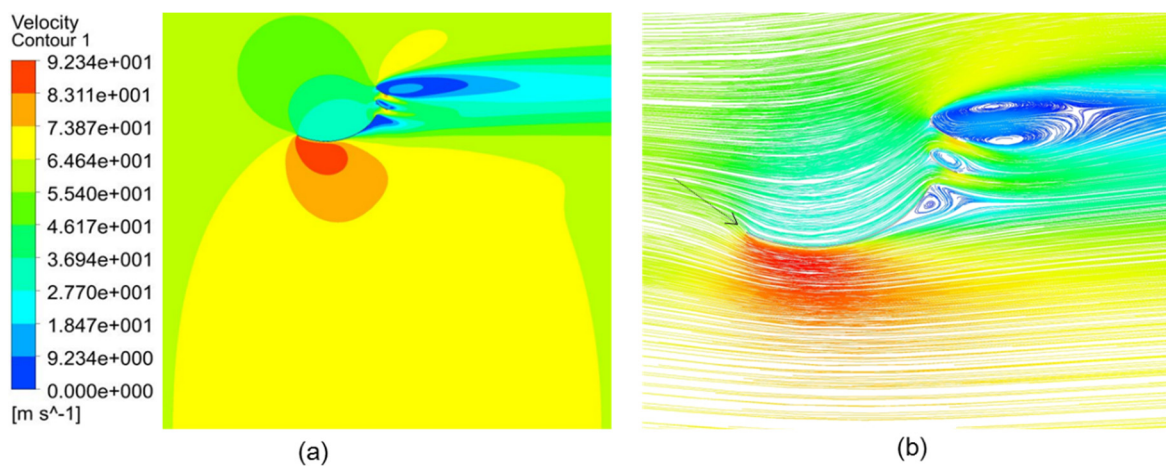


Figure 14. Flow fields around the diffuser with a bended self-adaptive flange at 60 m/s: (a) velocity contour and (b) streamline.

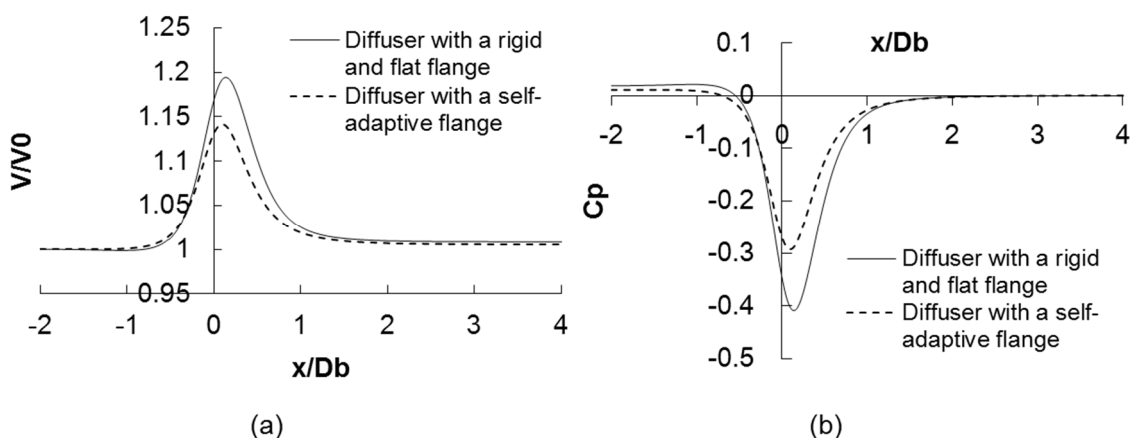


Figure 15. Distributions of streamwise velocity and pressure coefficient along the axisymmetric axis in the flanged diffusers with a rigid and flat and with a bended self-adaptive flange: (a) streamwise velocity and (b) pressure coefficient.

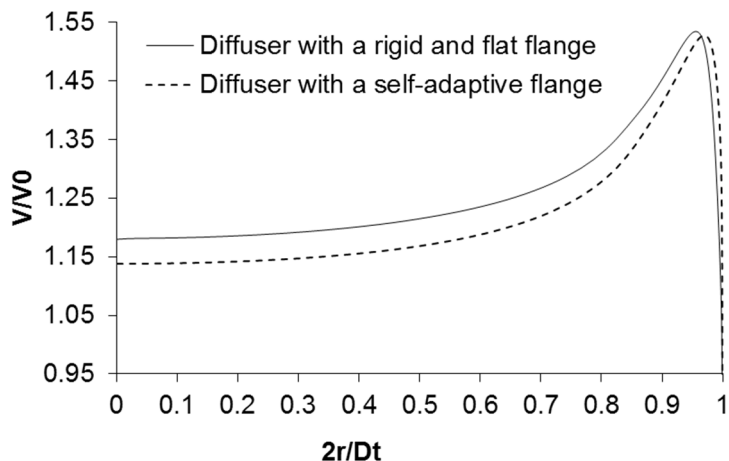


Figure 16. Distributions of wind velocity on the rotor planes, at 60 m/s, of two flanged diffusers with a rigid and flat flange and with a bended self-adaptive flange, respectively.

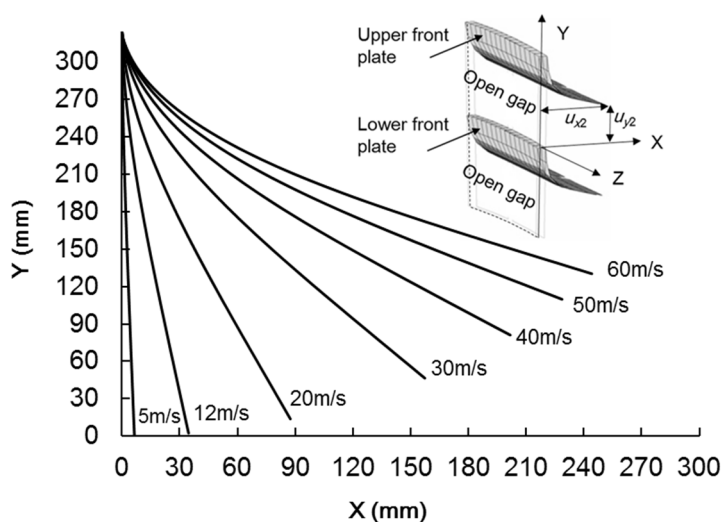


Figure 17. Configurations of deformed upper front plate of the self-adaptive flange at various wind velocities.

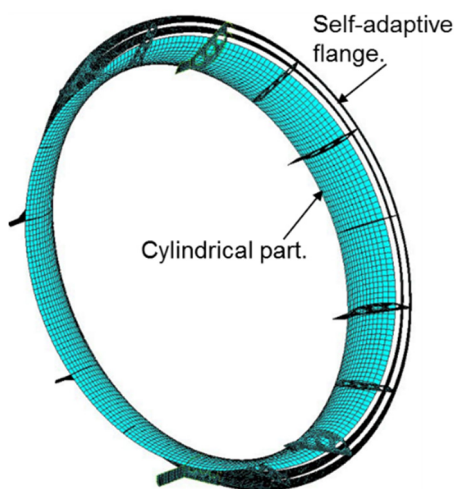


Figure 18. Full image of the diffuser with a self-adaptive flange at 60 m/s.

In Figure 15a,b the distributions of streamwise velocity and pressure coefficient along the axisymmetric axis in the flanged diffusers with a rigid and flat flange, and with a bended self-adaptive flange are depicted together for a comparison. Solid and dotted curves denote the results of the diffuser with a rigid and flat flange and those of the diffuser with a bent self-adaptive flange, respectively. The maximum velocity increment occurs near the rotor plane for the two kinds of flanged diffusers. It is seen that the maximum velocity increment and the absolute value of the pressure coefficient in the diffuser with a bended self-adaptive flange decrease by 27.87% and 28.5%, respectively, due to the deformation of the self-adaptive flange, compared to those in the diffuser with a rigid and flat flange. To demonstrate the distribution of wind velocity along the radial direction of the flanged diffuser, the distributions of wind velocity on the rotor planes, at 60 m/s, of two flanged diffusers with a rigid and flat flange and with a bended self-adaptive flange are depicted in Figure 16, respectively. It is seen that slow increase in the wind velocities in the rotor planes of two kinds of flanged diffuser is seen in the region of $2r/D_t < 0.6$ and fast increase is seen near the wall of the diffuser. These results are consistent with those shown in Figure 13a and Figure 14a. Furthermore, it is again seen that the wind velocity in the rotor plane of the diffuser with a self-adaptive flange is lower than that in the rotor plane of the flanged diffuser with a rigid and flat flange, except for a very small region near the wall of the diffuser. These results again confirm the availability of the self-adaptive flange for the reduction in the wind load acting on the flanged diffuser and wind turbine blades at high wind velocities.

Figure 17 presents the configurations of the deformed upper front plate of the self-adaptive flange under various velocities. The small draft in the upper-right of the figure shows an image of the self-adaptive flange at 60 m/s. It should be noted that the deformation of the lower front plate of the self-adaptive is similar to that of the upper front plate because of the similar geometry and the same boundary conditions. It can be seen that at the rated velocity of 12 m/s the displacement of free end of the plate is 34.6 mm in the X direction which is close to the gap (35 mm) between the front and rear plates. That is, the front plate almost touches the rear plate at the rated velocity. After that, the gaps in both directions of X and Y increase and the open gap in Y direction reaches 130 mm at 60 m/s. A full image of the flanged diffuser with a self-adaptive flange at 60 m/s is presented in Figure 18. The deformation of the self-adaptive flange creates two ring-like open gaps. As a result, much more wind can flow through the gaps so that the wind loads acting on the flange and the wind turbine blades decrease at high velocities. Numerical results related to the drags acting on the flanged diffuser, on the cylindrical part, and on the self-adaptive flange are depicted in Figure 19. Here, F_d denotes a drag and F_{d-0} denotes the drag acting on the diffuser with a rigid and flat flange. Solid line shows the drag ratio of the total drag acting on the diffuser with a self-adaptive flange over F_{d-0} , dotted curve with triangle marks shows the drag ratio for the flange part, and dashed curve with diamond marks gives the drag ratio for the cylindrical part. It is seen that the drag ratio of the cylindrical part decreases slightly with the increase of wind velocity, which is reasonable because the cylindrical part is assumed as rigid part and does not deform. Besides, it is seen that the drag ratios show almost no decrease at wind velocities below 12 m/s. These results further confirm that the self-adaptive flange can maintain the acceleration function at the wind velocities below the rated velocity. On the other hand, the values of drag ratio of the whole flanged diffuser and the flange decrease significantly from 0.996 to 0.65 and 0.618 to 0.341, respectively, with the increase of the wind velocity from 12 to 60 m/s. The wind loads acting on the whole flanged diffuser, on the flange, and on the cylindrical part are reduced by about 34.5%, 45.1%,

and 18.4%, respectively, due to the deformation of self-adaptive flange at 60 m/s. These results further prove that the present proposed diffuser with a self-adaptive flange is available for the reduction of the wind load acting on the flanged diffuser and is applicable for the middle and large-scale wind turbines with a flanged diffuser.

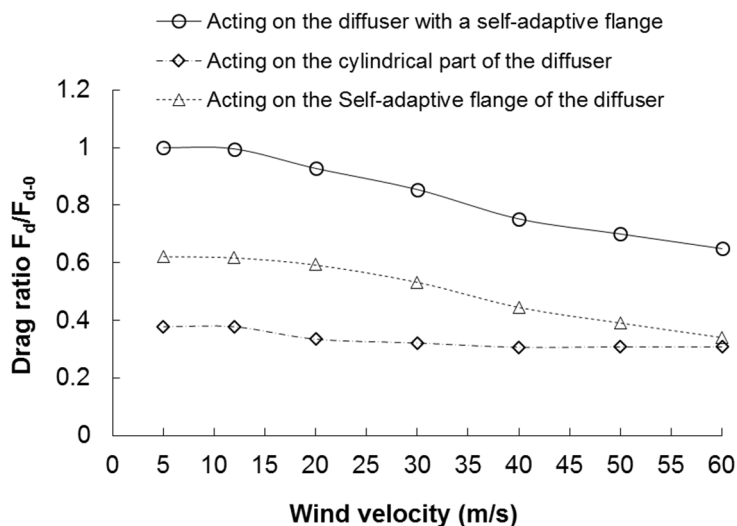


Figure 19. Drag ratio of the diffuser with a self-adaptive flange at various wind velocities.

5. Conclusions

In this study, a self-adaptive flange is proposed for the wind turbine shrouded by a flanged diffuser to reduce the wind loads acting on the flanged diffuser at high wind velocities. The self-adaptive flange can maintain the advantages of the flanged diffuser at wind velocities lower than the rated velocity and reduce the wind load acting on the diffuser and blades at higher wind velocities. Numerical analyses of fluid–structure interaction between the flow and the diffuser with a self-adaptive flange are carried out to investigate the flow field around the flanged diffuser and the variation of wind load acting on the flanged diffuser due to the reconfiguration of self-adaptive flange at various wind velocities. Based on the above numerical analyses and discussions the following conclusions are obtained:

1. About 60% of the total wind load acting on the total flanged diffuser of a wind turbine shrouded by a typical compact flanged diffuser is caused by the wind load acting on the flange. Therefore, reduction of the wind load acting on the flange is important in the development of middle and large scale wind turbines shrouded by a flanged diffuser.
2. The presented self-adaptive flange without any extra energy consumption is a viable solution. The structure of the self-adaptive flange is rather simple and practically feasible for the application to the middle and large scale wind turbines shrouded by a flanged diffuser to reduce the wind load acting on the wind turbine structure at high velocities.
3. The presented numerical results demonstrate that the wind load acting on the total flanged diffuser can be reduced by about 34.5% using the proposed self-adaptive flange. Furthermore, the reduction in the wind loads acting on the wind turbine blades is also expectable at high wind velocities beyond the rated value since the wind velocity in the rotor plane is reduced due to the deformation of the self-adaptive flange.

4. Manufacturing tests of the proposed diffuser with a self-adaptive flange and wind tunnel experiments using an actual wind turbine shrouded by the diffuser with a self-adaptive flange are needed to further confirm the feasibility in practice.
5. Further simulations considering the presence of the rotor are necessary in future research.

Acknowledgments

The authors gratefully acknowledge the help of Terutake Matsubara of the Research Institute for Applied Mechanics, Kyushu University, for his useful advice in this research.

Author Contributions

Jun Feng Hu conducted the iterative simulations of FEM and CFD and wrote the article. Wen-Xue Wang proposed the basic idea and supervised the simulations.

Conflicts of Interest

The authors declare no conflict of interest.

References

1. Lilley, G.M.; Rainbird, W.J. *A Preliminary Report on the Design and Performance of Ducted Windmills*; Report 102; College of Aeronautics Cranfield: Cranfield, UK, 1956.
2. Oman, R.A.; Foreman, K.M.; Gilbert, B.L. A progress report on the diffuser augmented wind turbine. In Proceedings of the 3rd Biennial Conference and Workshop on Wind Energy Conversion Systems, Washington, DC, USA, 8–12 June 1975; pp. 829–826.
3. Igra, O. Research and development for shrouded wind turbines. *Energy Convers. Manag.* **1981**, *21*, 13–48.
4. Igra, O. Compact shrouds for wind turbines. *Energy Convers. Manag.* **1977**, *16*, 149–157.
5. Foreman, K.M.; Gilbert, B.; Oman, R.A. Diffuser augmentation of wind turbines. *Solar Energy* **1978**, *20*, 305–311.
6. Phillips, D.G.; Richards, P.J.; Flay, R.G.J. CFD modelling and the development of the diffuser augmented wind turbine. *Wind Struct.* **2002**, *5*, 267–276.
7. Hansen, M.O.L.; Sørensen, N.N.; Flay, R.G.J. Effect of placing a diffuser around a wind turbine. *Wind Energy* **2000**, *3*, 207–213.
8. Bet, F.; Grassmann, H. Upgrading conventional wind turbines. *Renew. Energy* **2003**, *28*, 71–78.
9. Jafari, S.A.H.; Kosasih, B. Flow analysis of shrouded small wind turbine with a simple frustum diffuser with computational fluid dynamics simulations. *J. Wind Eng. Ind. Aerodyn.* **2014**, *125*, 102–110.
10. Van Bussel, G.J.W. The science of making more torque from wind: Diffuser experiments and theory revisited. *J. Phys. Conf. Ser.* **2007**, *75*, doi:10.1088/1742-6596/75/1/012010.
11. Werle, M.J.; Presz, W.M. Ducted wind/water turbines and propellers revisited. *J. Propuls. Power* **2008**, *24*, 1146–1150.

12. Jamieson, P.M. Beating Betz: Energy Extraction Limits in a Constrained Flow Field. *J. Sol. Energy Eng.* **2009**, *131*, 031008.
13. Ohya, Y.; Karasudani, T.; Sakurai, A.; Inoue, M. Development of high-performance wind turbine with a brimmed diffuser—Part 1. *Jpn. Soci. Aeronaut. Space Sci.* **2003**, *50*, 477–482.
14. Ohya, Y.; Karasudani, T.; Sakurai, A.; Inoue, M. Development of high-performance wind turbine with a brimmed diffuser—Part 2. *Jpn. Soc. Aeronaut. Space Sci.* **2004**, *52*, 210–213.
15. Abe, K.; Ohya, Y. An investigation of flow fields around flanged diffusers using CFD. *J. Wind Eng. Ind. Aerodyn.* **2004**, *92*, 315–330.
16. Abe, K.; Nishida, M.; Sakurai, A.; Ohya, Y.; Kihara, H.; Wada, E.; Sato, K. Experimental and numerical investigations of flow fields behind a small wind turbine with a flanged diffuser. *J. Wind Eng. Ind. Aerodyn.* **2005**, *92*, 951–970.
17. Ohya, Y.; Karasudani, T.; Sakurai, A.; Abe, K.I.; Inoue, M. Development of a shrouded wind turbine with a flanged diffuser. *J. Wind Eng. Ind. Aerodyn.* **2008**, *96*, 524–539.
18. Ohya, Y.; Karasudani, T. A shrouded wind turbine generating high output power with wind-lens technology. *Energies* **2010**, *3*, 634–649.
19. Mansour, K.; Meskinkhoda, P. Computational analysis of flow fields around flanged diffusers. *J. Wind Eng. Ind. Aerodyn.* **2014**, *124*, 109–120.
20. Wang, W.X.; Matsubara, T.; Hu, J.F.; Odahara, S.; Nagai, T.; Karasutani, T.; Ohya, Y. Experimental investigation into the influence of the flanged diffuser on the dynamic behavior of CFRP blade of a shrouded wind turbine. *Renew. Energy* **2015**, *78*, 386–397.
21. Takada, Y. Application of Wind Lens to the Large-Scale Windmill. Master's Thesis, Department of Aeronautics and Astronautics, Engineering School, Kyushu University, Fukuoka, Japan, 2009.
22. Lee, J.S.; Lee, S.H. Fluid–structure interaction analysis on a flexible plate normal to a free stream at low Reynolds numbers. *J. Fluids Struct.* **2012**, *29*, 18–34.
23. Bai, X.; Avital, E.J.; Munjiza, A.; Williams, J.J.R. Numerical simulation of a marine current turbine in free surface flow. *Renew. Energy* **2014**, *63*, 715–723.
24. Jones, R.M. *Mechanics of Composite Materials*; Scripta Book Company: New York, NY, USA, 1975; pp. 147–236.
25. Homicz, G.F. *Computational Fluid Dynamic Simulations of Pipe Elbow Flow*; Sand Report Sand 2004–3467; Sandia National Laboratories: Albuquerque, NM, USA, 2004; pp. 1–40.